Technology in Cancer Research and Treatment
ISSN 1533-0346
Volume 11, Number 4, August 2012

Macromolecular Changes in Nilotinib Resistant K562 Cells; an *In vitro* Study by Fourier Transform Infrared Spectroscopy

Cagatay Ceylan, Ph.D.[1]*
Aylin Camgoz, M.Sc.[2]
Yusuf Baran, Ph.D.[2]*

[1]İzmir Institute of Technology, Department of Food Engineering, Urla, İzmir, Turkey
[2]İzmir Institute of Technology, Department of Molecular Biology and Genetics, Urla, İzmir, Turkey

www.tcrt.org

Nilotinib is a second generation tyrosine kinase inhibitor which is used in both first and second line treatment of chronic myeloid leukemia (CML). In the present work, the effects of nilotinib resistance on K562 cells were investigated at the molecular level using Fourier transform infrared (FT-IR) spectroscopy. Human K562 CML cells were exposed to stepwise increasing concentrations of nilotinib, and sub-clones of K562 cells resistant to 50 nM nilotinib were generated and referred to as K562/NIL-50 cells. Antiproliferative effects of nilotinib were determined by XTT cell proliferation assay. Changes in macromolecules in parental and resistant cells were studied by FT-IR spectroscopy. Nilotinib resistance caused significant changes which indicated increases in the level of glycogen and membrane/lipid order. The amount of unsaturated lipids increased in the nilotinib resistant cells indicating lipid peroxidation. The total amount of lipids did not change significantly but the relative proportion of cholesterol and triglycerides altered considerably. Moreover, the transcriptional status decreased but metabolic turn-over increased as revealed by the FT-IR spectra. In addition, changes in the proteome and structural changes in both proteins and the nucleus were observed in the K562/NIL-50 cells. Protein secondary structural analyses revealed that alpha helix structure and random coil structure decreased, however, anti-parallel beta sheet structure, beta sheet structure and turns structure increased. These results indicate that the FT-IR technique provides a method for analyzing drug resistance related structural changes in leukemia and other cancer types.

Key words: Nilotinib; Chronic myeloid leukemia (CML); Tyrosine kinase inhibitor resistance; Fourier transform infrared spectroscopy (FT-IR).

Introduction

Nilotinib is one of the most common second generation tyrosine kinase inhibitors used in the treatment of chronic myeloid leukemia (CML) (1). CML results from a reciprocal translocation between the long arms of chromosomes 9 and 22. This exchange generates a BCR-ABL fusion gene that encodes an oncoprotein having constitutive tyrosine kinase activity. The oncoprotein activates signal transduction pathways, leading to uncontrolled cell growth and reduced apoptosis (2). Nilotinib not only inhibits the kinase activity of the BCR-ABL protein, but also inhibits c-KIT and platelet-derived growth factor (PDGFR) (3). Nilotinib is a very effective drug in the treatment of imatinib (the first generated and applied tyrosine kinase inhibitor for CML) resistant and intolerant patients (4). However,

Abbreviations: CML: Chronic Myeloid Leukemia; FT-IR: Fourier Transform Infrared; K562/NIL-50: K562 Cells Resistant to 50 nM Nilotinib; PDGFR: Platelet-derived Growth Factor Receptor; PBS: Phosphate Buffered Saline.

*Corresponding authors:
Assistant Prof. Dr. Cagatay Ceylan, Ph.D.
Phone: +90 232 750 6328
Fax: +90 232 750 6196
E-mail: cagatayceylan@iyte.edu.tr
Associate Prof. Dr. Yusuf Baran, Ph.D.
Phone: +90 232 7507515
Fax: +90 232 7507509
E-mail: yusufbaran@iyte.edu.tr

resistance to nilotinib was recently observed in CML (5, 6). Such resistance remains a significant impediment to successful tyrosine kinase inhibitor therapy in CML treatment.

Fourier transform infrared spectroscopy is a rapid, sensitive and nondestructive method which is widely used in the analysis of biological systems in any physical state, and can be used to monitor molecular changes (7, 8). The method requires only minute amounts of sample and allows analysis of the data with many different digital manipulations. It is a valuable analytical technique for simultaneous detection of changes in cellular components such as lipids, proteins, carbohydrates and nucleic acids at the level of functional groups. The technique qualitatively and quantitatively evaluates shifts in peak positions, changes in bandwidths and band intensities to obtain structural and functional information about the systems analyzed. In addition, FTIR spectroscopy provides information about the amount and chemical and physical nature of the groups in close vicinity (7-9).

An FT-IR spectrum is a molecular fingerprint of the studied tissue or cells, therefore the technique can be used to follow the effects of biological differentiation processes. Disease processes are examples of such differentiation processes during which significant metabolic changes occur in the cell. These metabolic changes result in alterations in carbohydrate, lipid and protein profiles, hence changes in the macromolecular composition of the cells of interest. In addition to its use in the chemical and food industries, FT-IR technique has been developed to be a valuable diagnostic tool to analyze and detect various disease conditions including cancer (10, 11).

In this study, we developed nilotinib resistant sublines of BCR-ABL positive K562 CML cells and examined the possible roles of macromolecules in nilotinib resistance by Fourier Transform Infrared Spectroscopy (FT-IR). For this purpose, nilotinib resistant K562 cells were generated. Although resistance-dependent macromolecular changes in K562 cells against different anti-cancer drugs have been investigated using FT-IR technique (12, 13), this is the first biochemical variations between sensitive and K562/NIL-50 cells were compared.

Materials and Methods

Cell Lines and Culture Conditions

K562 CML parental cells were obtained from the German Collection of Microorganisms and Cell Cultures (Germany). The cells were cultured in RPMI-1640 growth medium (Biological Industries, Israel) containing 15% fetal bovine serum (Biological Industries, Israel) and 1% penicillin-streptomycin (Biological Industries, Israel) at 37 °C in 5% CO_2. The medium was refreshed every 3 days. The cell suspension was taken from tissue culture flasks into a sterile falcon tube and was centrifuged for 10 minutes at 1000 rpm. The supernatant was removed and the pellet washed with 2 milliliters of phosphate buffered saline (PBS). The cells were recentrifuged at 1000 rpm for 10 minutes. The cells were resuspended in 15 milliliters of RPMI-1640 medium and transferred into sterile culture flasks.

Generation of Nilotinib Resistant K562 Cells

K562 CML cells were exposed to step-wise increasing concentrations of nilotinib, kindly provided by Novartis, starting with a concentration of 1 nM. Sub-clones of K562 cells that were able to survive and grow in the presence of 50 nM nilotinib were generated and referred to as K562/NIL-50 cells.

Measurement of Cell Proliferation by XTT Assay

The IC50 value of nilotinib in K562 and K562/NIL-50 cells were determined for both parental and resistant cells as previously described (14). Before doing all the experiments, we conducted trypan blue dye exclusion assay in order to make it sure that all the cells were alive. In XTT assay, 2×10^4 cells/well were seeded into 96-well plates containing 200 µl of the growth medium with increasing concentrations of nilotinib and incubated at 37 °C in 5% CO_2. Following an incubation period of 72 hours, the cells were exposed to 50 µl XTT reagent (Biological Industries, Israel) for 4 hours. Finally, readings were carried out at 492 nm in an Elisa reader (Thermo Electron Corporation Multiskan Spectrum, Finland) and the IC50 value of nilotinib was calculated from the cell proliferation plots.

Sample Preparation for FT-IR Spectroscopy

We used 5×10^6 cells grown in 15 ml RPMI-1640 medium. The cells were collected, dissolved in sterile distilled water and lyophilized in a freeze drier (Labconco, FreeZone 18 liter freeze dry system) overnight to remove water. The cell powder was mixed with dried potassium bromide (KBr) (Sigma-Aldrich, USA) in a mortar (at a ratio of 1:100). The mixture was then pressurized to 100 kg/cm^2 (1200 psi) for 5 minutes. All the cell growth, cell collection and FT-IR experiments for the sensitive and nilotinib resistant K562 cells were performed on the same day.

FTIR Spectrum Accumulation and Data Processing

The spectral analysis was carried out using a Perkin-Elmer spectrometer equipped with MIR TGS detector (Spectrum 100 Instrument, Perkin Elmer Inc., Norwalk, CT, USA). FTIR spectra of the samples were recorded between 4000 and 450 cm^{-1}. Interferograms were averaged for 20 scans at 4 cm^{-1} resolution. The background spectrum was

automatically subtracted from the spectra of the samples. Spectrum 100 software (Perkin Elmer) was used for all data manipulations.

From each sample, at least three different scans, which gave identical spectra, were performed. These replicates (n = 10 for the sensitive; n = 5 for the resistant cells) were averaged and the averaged spectra for each sample were then used for further data manipulation and statistical analysis. The spectra were smoothed over 19 points using the Savitsky-Golay algorithm. Then, the spectra were interactively baselined from two arbitrarily selected points. Finally, the spectra were normalized in specific regions for visual comparison of the nilotinib sensitive and resistant samples.

For the determination of protein secondary structural changes the second derivative spectra were obtained by applying a Savitzky-Golay algorithm with five points. The second derivatives were normalized between 1700 and 1600 cm^{-1} and the peak intensities were calculated. The peak minima of the second derivative signals were considered because they correspond to the peak maxima of the original absorption spectra (15).

Statistical Analysis: The differences between the nilotinib-sensitive and resistant groups were compared using the Mann-Whitney U Test with the Matlab R2010b program. The statistical results are expressed as means ± standard deviation. $p < 0.05$ was considered statistically significant.

Results

Antiproliferative Effects of Nilotinib on K562 and K562/NIL-50 Cells

In order to determine the resistancy of K562/NIL-50 cells to nilotinib, K562 and K562/NIL-50 cells were exposed to increasing concentrations of nilotinib for 72 hours. The IC50 value of nilotinib was calculated to be 42- and 385 nM for K562 (Figure 1A) and K562/NIL-50 cells (Figure 1B). The results revealed that K562/NIL-50 cells were at least 9-fold more resistant to nilotinib when compared to its parental sensitive counterparts.

FT-IR Studies

Since the FTIR spectroscopy technique provides useful information about the structure and function of the macromolecular constituents of biological systems at the molecular level (7-9), the technique was used in the analysis of the effects of nilotinib resistance on K562 cells in our studies.

Figure 2 shows the average FTIR spectra of control K562 cells in the 3700-950 cm^{-1} spectral region. Assignments of the major bands in Figure 2 are presented in Table I. Because

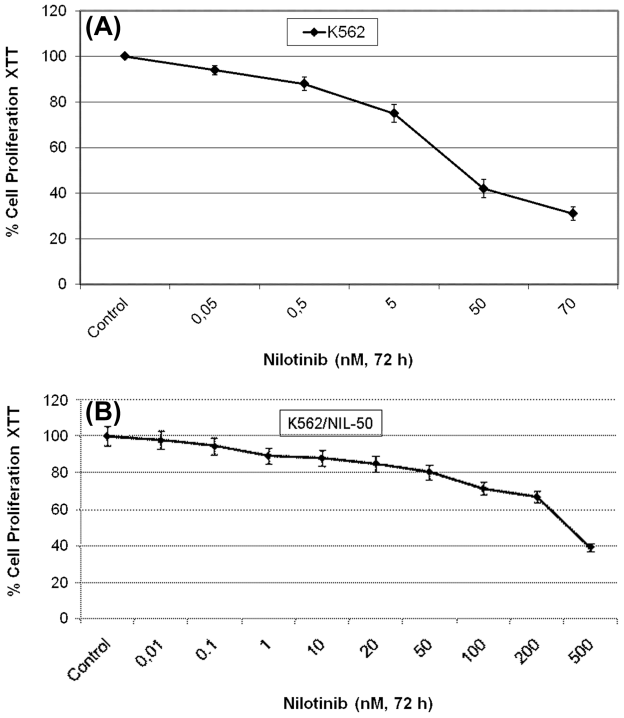

Figure 1: Effects of nilotinib on growth of (**A**) K562 and (**B**) K562/NIL-50 cells. Cytotoxicity was determined by the XTT cell proliferation test in a 72 h culture. The IC50 concentration of Nilotinib was calculated from cell proliferation plots. The XTT assays were performed using triplicate samples in at least three independent experiments. The error bars represent the standard deviations ($p < 0.05$).

the FTIR spectrum of cancer cells is quite complex and consists of several bands originating from the contribution of different functional groups belonging to biomolecules, such as lipids, proteins and nucleic acids, the spectra were analyzed for the following regions: 2840-3700 cm^{-1} for the analysis of proteins and lipids, and 1480-1800 cm^{-1} for the analysis of proteins and lipids, 940-1480 cm^{-1} for the analysis of the fingerprint region. All the spectra presented in the figures were

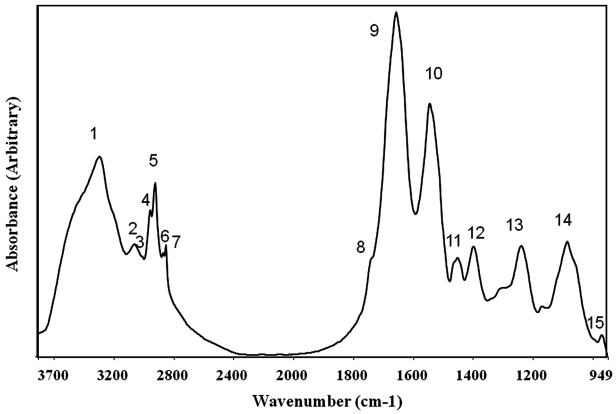

Figure 2: The general FT-IR spectrum of K562 cells in 3700-930 cm^{-1} region.

Table I
The general FTIR band assignments of K562 cells.

Band number	Wave numbers (cm^{-1})	Definition of the spectral assignment
1	3299	Amide A: Mainly N-H stretching of proteins with the little contribution from O-H stretching of polysaccharides and intermolecular bonding.
2	3063	Amide B: C-N and N-H stretching of proteins.
3	3015	Olefinic =CH stretching vibration: unsaturated lipids, cholesteryl esters.
4	2959	CH_3 asymmetric stretching: lipids, protein side chains, with some contribution from carbohydrates and nucleic acids.
5	2925	CH_2 asymmetric stretching: mainly lipids, and the little contribution from proteins, carbohydrates and nucleic acids.
6	2872	CH_3 symmetric stretching: protein side chains, lipids, with some contribution from carbohydrates and nucleic acids.
7	2854	CH_2 symmetric stretching: mainly lipids, with the little contribution from proteins, nucleic acids and carbohydrates.
8	1743	Ester C=O stretching: triglycerides and cholesterol esters.
9	1657	Amide I: proteins, mainly C=O stretch.
10	1545	Amide II: proteins, mainly N-H bend and C-N stretch.
11	1452	CH_2 bending: mainly lipids, with the little contribution from proteins, CH_3 asymmetric bending methyl groups of proteins.
12	1399	COO^- symmetric stretching: mainly lipids with the little contribution from proteins; CH_3 symmetric bending: methyl groups of proteins.
13	1239	PO_2^- asymmetric stretching, fully hydrogen bonded: mainly nucleic acids with the little contribution from phospholipids.
14	1086	PO_2^- symmetric stretching: nucleic acids and phospholipids; C-O stretch glycogen.
15	970	$C\text{-}N^+\text{-}C$ stretching: nucleic acids.

normalized with respect to specific selected bands and are used only for illustrative purposes. However, in the measurement of the spectral parameters, each original baseline-corrected spectrum belonging to the corresponding nilotinib-sensitive and resistant groups was considered separately.

2840-3700 cm^{-1} Region

Figure 3 shows the average FTIR spectra of the sensitive and K562/NIL-50 cells in the 2840-3700 cm^{-1} spectral region. The FTIR spectrum in this region consists of Amide A band which has contributions from mainly the N-H stretching of proteins with a small contribution from the O-H stretching of polysaccharides and intermolecular H bonding (16); Amide B band which has contributions from C-N and N-H stretching of proteins; the olefinic =CH stretching vibration band located at 3010 cm^{-1}, which has contributions from cholesterol esters, the CH_3 asymmetric stretching band located at 2959 cm^{-1}, which has contributions from both lipids and proteins (8); the CH_2 asymmetric stretching band located at 2925 cm^{-1} which is mainly due to lipids (18); the CH_3 symmetric stretching band located at 2872 cm^{-1} which mainly monitors protein side chains with some contribution from lipids, carbohydrates and nucleic acids; and CH_2 symmetric stretching band located at 2854 cm^{-1} which monitors mainly lipids, with small contributions from proteins, nucleic acids and carbohydrates (17, 18).

As seen from Figure 3, nilotinib resistance induced remarkable changes in the bandwidth, intensity and frequency value of the FT-IR bands in this region. Comparisons of the band intensities of some infrared bands of nilotinib sensitive and resistant K562 cells are shown in Figure 4. In addition the

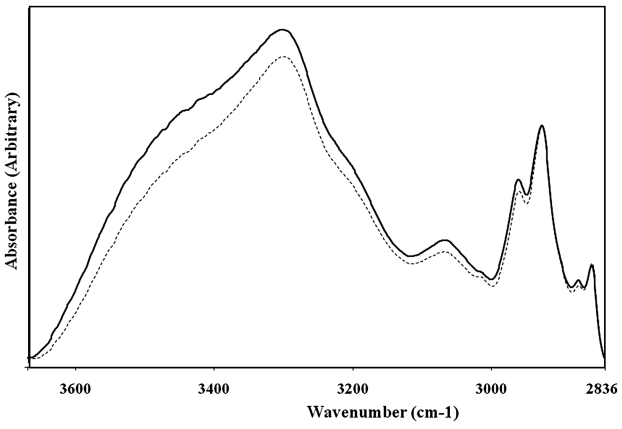

Figure 3: The FT-IR spectra of nilotinib sensitive (solid line) and resistant (dotted line) cells in the 3666-2836 cm^{-1} region (the spectra were normalized with respect to CH_2 asymmetric mode, which is observed at 2925 cm^{-1}).

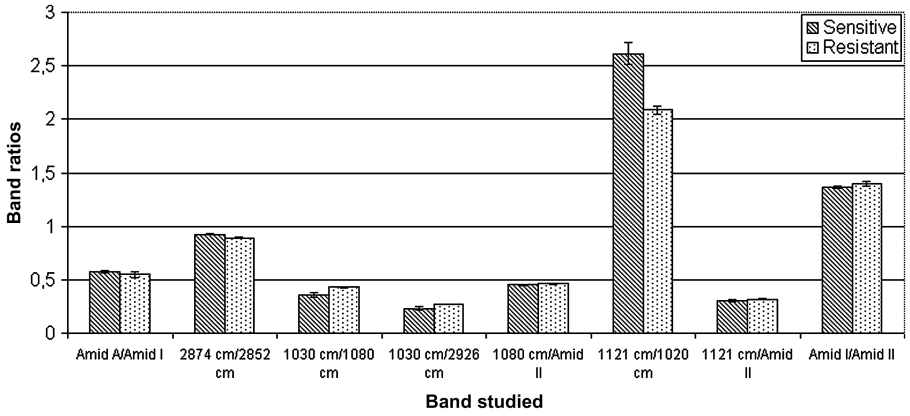

Figure 4: The intensity-ratio values of the bands for nilotinib sensitive and resistant K562 cells. The values are the mean +/− standard deviation for each group.

intensity ratios are given in Table II. As can be seen from Figure 3 there was a significant reduction in the intensity of amide A and amide B bands, which are located at 3299 cm^{-1} and 3063 cm^{-1} respectively, which contains strong absorptions arising mainly from N-H stretching mode of proteins with the contribution of the O-H stretching mode of polysaccharides (16, 18-22) and intermolecular H bonding (23) of K562 cells. When normalized with the intensity of the Amide I band, the same reduction was observed for nilotinib resistant cells as seen in Figure 4. The intensity ratio of Amide A and Amide I decrease by 5.21% in K562/NIL-50 cells ($p = 0.0553$). In addition, the frequency of the Amid A band shifted from 3299.97 +/− 0.311 to 3298.34 +/− 1.765 cm^{-1} in K562/NIL-50 cells ($p = 0.0013$). However, the frequency of the Amide B band shifted from 3063.51 +/− 0.56 to 3064.38 +/− 2.98 cm^{-1} in nilotinib resistant K562 cells.

The region between 3020 cm^{-1} and 2833 cm^{-1} is populated by absorptions arising from C-H stretching vibrations of aliphatic compounds. The changes in the intensity of the band at 3015 cm^{-1}, which are due to the CH stretching mode of HC=CH groups, reflect the level of unsaturation in the acyl chains (24). For the nilotinib sensitive cells the unsaturation level of lipids based on the $CH{=}CH/CH_2$ ratio (25) was found to be 0.00517 +/− 0.000595 and for the nilotinib resistant cells the ratio was 0.01416 +/− 0.000344 ($p < 0.0001$). As seen in Figure 5 the intensity of the band at 3015 cm^{-1} increased for the K562/NIL-50 cells. When normalized to the band at 2925 cm^{-1}, the intensity of the CH_3 asymmetric band at 2959 cm^{-1} and CH_3 symmetric stretch band at 2872 cm^{-1} decreased for K562/NIL-50 cells, whereas the intensity of the CH_2 symmetric stretch band at 2854 cm^{-1} increased for K562/NIL-50 cells. In Figure 4 the intensity ratio of 2874 cm^{-1} and 2852 cm^{-1} decreased by 3.53% in K562/NIL-50 cells ($p < 0.001$). The frequency of the CH_3 asymmetric stretch band around 2958 cm^{-1} band shifted from 2959.1 +/− 0.065 to 2958.58 +/− 0.092 cm^{-1} in K562/NIL-50 cells ($p < 0.001$).

1480-1800 cm^{-1} Region

Figure 6 shows the average FTIR spectra of the sensitive and K562/NIL-50 cells in the 1800-1480 cm^{-1} spectral region. The FTIR spectrum in this region represents the well-known

Table II

The results of the changes in the intensity ratios of main bands for the nilotinib sensitive and resistant K562 cells.

	Band intensity ratio		
Functional groups	Nilotinib sensitive	Nilotinib resistant	*p* value
Amid A/Amid I	0.57669 +/− 0.01076	0.54805 +/− 0.0299	$p < 0.01$
2874 cm^{-1}/2852 cm^{-1}	0.9248 +/− 0.0026	0.892214 +/− 0.0055	$p < 0.005$
1030 cm^{-1}/1080 cm^{-1}	0.3542 +/− 0.0226	0.42851 +/− 0.00307	$p < 0.005$
1030 cm^{-1} /2926 cm^{-1}	0.2326 +/− 0.01358	0.2727 +/− 0.00266	$p < 0.005$
1080 cm^{-1}/Amid II	0.45021 +/− 0.0049	0.4642 +/− 0.00389	$p < 0.005$
1121 cm^{-1}/1020 cm^{-1}	2.6142 +/− 0.0995	2.0884 +/− 0.03645	$p < 0.005$
1121 cm^{-1}/Amid II	0.30317 +/− 0.0064	0.31589 +/− 0.00632	$p < 0.01$
Amid I/Amid II	1.3644 +/− 0.00915	1.3956 +/− 0.02518	$p < 0.05$

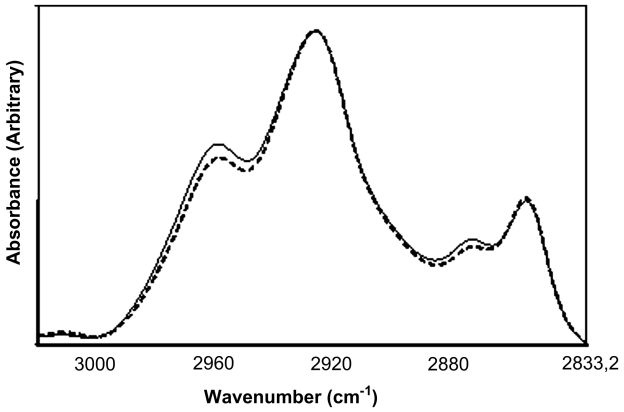

Figure 5: The FT-IR spectra of nilotinib sensitive (solid line) and resistant (dotted line) cells in the 3020-2836 cm^{-1} region (the spectra were normalized with respect to CH_2 asymmetric mode, which is observed at 2925 cm^{-1}).

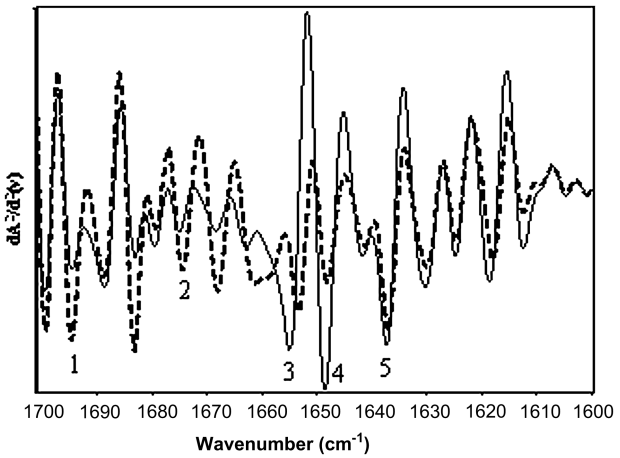

Figure 7: The average second derivative spectra of nilotinib sensitive (solid line) and resistant (dotted line) K562 cells in 1700-1600 cm^{-1} region.

amide I and amide II bands which have contributions from different protein secondary structural elements and the band centered at 1743 cm^{-1} which is mainly assigned to the C=O ester stretching vibration of triglycerides and cholesterol esters (7, 26, 27). As seen in Figure 6, the intensity and frequency of the C=O ester stretching vibration changed significantly. The bands at 1657 cm^{-1} and 1545 cm^{-1} are amide I and amide II bands of proteins. Amide I and Amide II bands are known to be sensitive to protein conformation (7) and are used to determine the secondary structure content of proteins. Changes in the shapes of these two bands indicated changes in the proteomes of the nilotinib resistant cells. In Figure 4 the ratio of the intensities of Amide I/Amide II bands increased (16.95%) for K562/NIL-50 cells ($p = 0.0193$). The structural changes in proteins were evaluated from the intensities of the sub-bands in Amide I secondary derivative spectra as seen in Figure 7. The assignments of the secondary structural components are given in Table III. The intensity values of the band are presented in Table IV. The results revealed that the alpha helical structure (located at 1653 cm^{-1}) decreased slightly in the nilotinib resistant cells ($p < 0.05$). Similarly, random coil structure (located at 1648 cm^{-1}) decreased significantly in the nilotinib resistant cells ($p < 0.001$). However the turns (located at 1674 cm^{-1}), the antiparallel beta sheet structure (located at 1694 cm^{-1}) increased significantly ($p < 0.001$). The beta sheet structure (located at 1637 cm^{-1}) also increased.

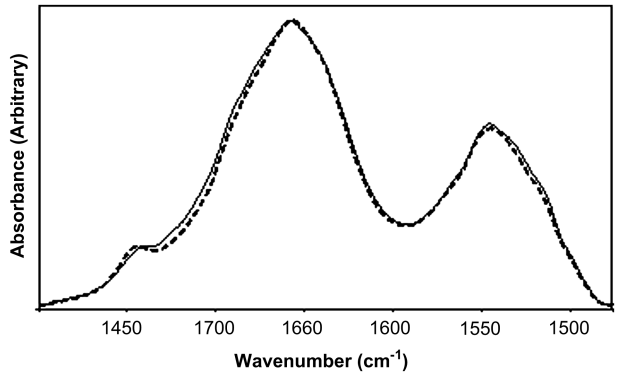

Figure 6: The FT-IR spectra of nilotinib sensitive (solid line) and resistant (dotted line) cells in the 1800-1480 cm^{-1} region (the spectra were normalized with respect to amide I band, which is observed at 1657 cm^{-1}).

940-1480 cm^{-1} (Fingerprint) Region

Figures 8A and 8B show the average FTIR spectra of the nilotinib sensitive and resistant K562 cells in the 940-1480 cm^{-1} spectral region. The bands in this spectral region have contributions from proteins, lipids, nucleic acids and carbohydrates. The band at 1452 cm^{-1} is attributed to CH_2 bending vibration of lipids (28, 29). The band at 1399 cm^{-1} is attributed to COO^- symmetric stretch of mainly lipids with a small contribution from proteins (29). The bands at 1239 and 1086 cm^{-1} are attributed to PO_2^- asymmetric and symmetric stretch of nucleic acids (30, 31). The band at 1155 cm^{-1} is attributed to C-O stretching of glycogen (32). A notable increase in the intensity of this band was observed in the K562/NIL-50 cells as seen in Figure 7B. The band at 970 cm^{-1} is assigned to C-N+-C stretch of nucleic acids (33). In the analysis of the band in this region the intensity ratio of the 1030 cm^{-1} and 1080 cm^{-1} bands increased by 21% in K562/NIL-50 cells ($p < 0.001$) as seen in Figure 4. Similarly, in the same figure the intensity ratio of 1030 cm^{-1} and 2926 cm^{-1} bands increased by 17.24% ($p < 0.001$); 1080 cm^{-1} and Amide II bands increased by 2.78% ($p < 0.001$) and 1121 cm^{-1} and Amide II bands increased by 5.18% ($p = 0.008$) in K562/NIL-50 cells. However, a considerable decrease (20.11%) in the intensity ratio of the 1121 cm^{-1} and 1020 cm^{-1} bands was observed in K562/NIL-50 cells ($p < 0.001$) as seen in Figure 4. In addition, the frequency of the band around 1453 cm^{-1}

Table III
The assignments of secondary structure sub-bands under Amide I band in 1700-1600 cm^{-1} region for nilotinib sensitive and resistant K562 cells (15).

Peak number	Mean frequencies (cm^{-1})	Assignment
1	1694	Anti-parallel beta sheet
2	1674	Turns
3	1653	Alpha helix
4	1648	Random Coil
5	1638	Beta sheet

shifted from 1452.66 +/− 0.236 to 1453.95 +/− 0.705 cm^{-1} in K562/NIL-50 cells as seen in Figure 7A ($p < 0.001$). However, in Figure 8B the frequency of the band around 1085 cm^{-1} band shifted from 1086.28 +/− 0.081 to 1085.35 +/− 0.042 cm^{-1} in K562/NIL-50 cells ($p < 0.001$).

Discussion

Targeting the tyrosine kinase activity of BCR-ABL is a common and attractive therapeutic strategy for the treatment of chronic myeloid leukemia. Nilotinib is a very effective tyrosine kinase inhibitor which gives positive results in both first and second line treatment of CML patients. Unfortunately, CML cells can somehow escape from the cytotoxic effects of nilotinib and gain resistance to nilotinib. This problem is the major obstacle for the successful treatment of CML. The molecular mechanisms of multidrug resistance in CML were shown by our group and other researchers (34, 35). However, changes in macromolecular levels in nilotinib resistant CML cells and the roles of these differences on nilotinib resistance were not examined and discussed in the literature. In this study, we investigate the changes in macromolecular structures between sensitive and nilotinib resistant CML cells by using Fourier Transform Infrared Spectroscopy and discuss possible outcomes. Overall, the study indicated that nilotinib resistance induces changes in the molecular structure of K562/NIL-50 cells as evidenced by changes in the intensity and frequency of the FTIR spectra.

In this study, water was removed from the samples in the sample preparation steps using lyophilization procedures. Although it was reported that dehydration can change the absorption characteristics of cells significantly, the studies were acceptable as long as the cells were always dried (36). In addition when the comparison of drug resistance states is investigated dried systems can provide comparative spectral data especially when the hydration levels of the both states are the same. In this study since water was essentially removed from the samples, water's contribution to Amid A, Amid B, Amid I and Amid II bands was negligible. For this reason, the 3299 cm^{-1} band can be considered to be due to only proteins and polysaccharides. The reduction in the intensity ratios of Amid A to Amid I in the nilotinib resistant cells cannot be due to the reduced contribution of glycogen since a significant increase was observed in the intensity of the 1155 cm^{-1} band which is mainly assigned to the C-O stretching vibrations in glycogen (32). Therefore, the reduction in the intensity of these two bands could be ascribed to a reduced contribution of polysaccharides in the resistant cells. Cancer cells are known to consume more carbohydrate due to their increased energy expenditure which is known as the Warburg Effect (37). In a similar way, MDR resistance is hypothesized to require more energy for the additional tasks of elimination of toxic compounds and drugs. In addition the conditions of hypoxia are induced in MDR in some cancer cell types (38, 39) and glycogen accumulation is known to occur in hypoxia (40).

As seen in Figure 5, the intensity of the band at 3015 cm^{-1} which is due to CH stretching of olefinic HC=CH stretching vibrations indicates that the population of unsaturated lipids increased in the resistant cells. The increase in the intensity of this band indicates a change in phospholipid metabolism.

Table IV
The results of the changes in the intensities of main protein secondary structures for nilotinib sensitive and resistant K562 cells.

Functional groups	Sensitive	Resistant	*p* values
Alpha helical structure (located at 1653 cm^{-1})	−0.90262 +/− 0.0678	−0.8639 +/− 0.02019	$p < 0.05$
Turns (located at 1674 cm^{-1})	−0.5834 +/− 0.0273	−0.6988 +/− 0.0259	$p < 0.001$
Antiparallel beta sheet structure (located at 1694 cm^{-1})	−0.6665 +/− 0.0130	−0.9566 +/− 0.05984	$p < 0.001$
Random coil structure (located at 1648 cm^{-1})	−0.9948 +/− 0.0102	−0.7486 +/− 0.0448	$p < 0.001$
Beta sheet structure (located at 1637 cm^{-1})	−0.8757 +/− 0.0195	−0.92146 +/− 0.0823	$p > 0.05$

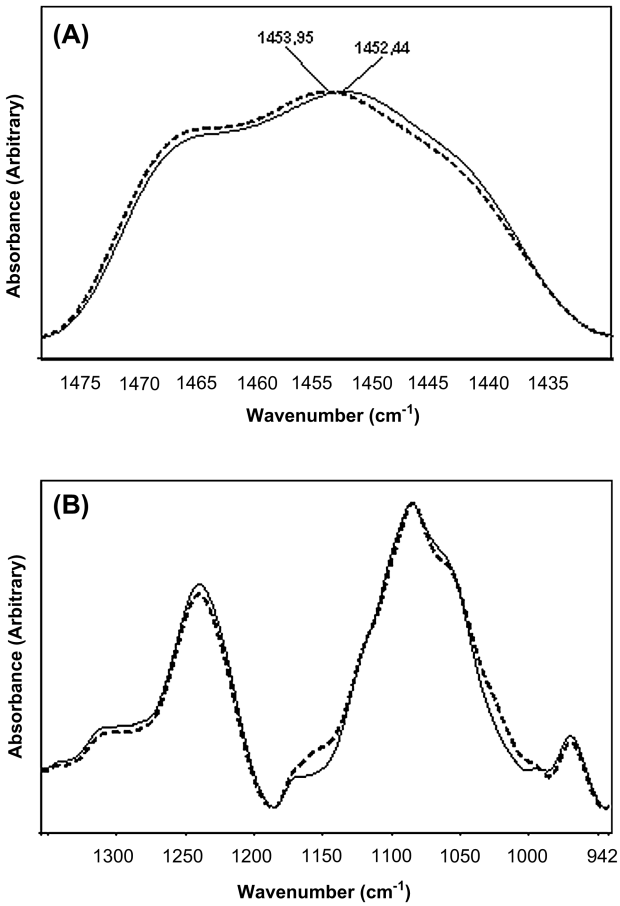

Figure 8: The FT-IR spectra of nilotinib sensitive (solid line) and resistant (dotted line) cells (**A**) in the 1480-1430 cm^{-1} region (the spectra were normalized with respect to CH_2 bending mode, which is observed at 1452 cm^{-1}), (**B**) in the 1350-930 cm^{-1} region (the spectra were normalized with respect to PO_2^- symmetric stretching mode, which is observed at 1086 cm^{-1}).

In addition the increase in the olefinic band may be due to the accumulation of end products of lipid peroxidation (41). The unsaturation level for the resistant cells was found to be 2.7389 times more that that of the nilotinib sensitive cells. This conclusion is supported by the results obtained from the bands around 1743 cm^{-1}. The change in shape and frequency of the band around 1743 cm^{-1} indicated the changes in the ratio of triglycerides and cholesterol esters and their saturation states. In Figure 6 it is seen that in K562/NIL-50 cells, the maximum of the band shifts to higher frequency values and the intensity also increases at around 1745 cm^{-1}.

In Figure 4 a decreased CH_3 asymmetric stretching vibration absorption intensity was observed in the resistant cells indicating a change in the composition of the acyl chains in lipids (24). In addition, the frequency of the CH_3 asymmetric stretch band shifted from 2959.1 to 2958.58 cm^{-1} in K562/NIL-50 cells. Since, the CH_3 asymmetric stretching mode is correlated with the order of the deep interior of the membrane, a decrease in the frequency corresponds to decreasing freedom of the acyl chain in the center of the bilayer (19). Therefore this result indicates that the order in the lipid membrane interior is increased in the resistant cells. In general plasma membrane order was found to be at a higher level when compared with drug sensitive counterparts (42). The drug resistant cells are known to have more ordered lipid domains (43). This may be due to the change in the fatty acid composition of the plasma membrane. In general the transport of anti-cancer drugs is carried out by special protein pumps located in the cell membranes. However since many of these drugs are hydrophobic in nature the order may influence the direct transport of these drugs from cell membrane. Therefore it is difficult to correlate the membrane order and drug resistance in a one-to-one relationship. In addition to changes in the CH_3 asymmetric stretching mode, the intensity of the CH_2 symmetric stretching band increased in the resistant cells indicating an increasing proportion of the CH_2 groups in the resistant cells. Similarly, the frequency of the bending vibration at 1452 cm^{-1} shifted from 1452.66 to 1453.95 cm^{-1} in K562/NIL-50 cells indicating changes in the lateral packing property of the methylene groups in the membrane lipids (44). A precise protein-to-lipid ratio can be derived by calculating the area ratio of the CH_3 symmetric stretching (2874 cm^{-1}) to the CH_2 symmetric stretching vibration (2852 cm^{-1}) from the FT-IR spectra (7). The intensity ratio of 2874 cm^{-1} and 2852 cm^{-1} was found to decrease by 3.53% in K562/NIL-50 cells. These results indicate a small increase in the lipid content of the cellular material for constant protein content or vice versa. There have been contrasting reports of the change in the amount of lipids in drug resistant cells (45, 46). In the study (12) the development of MDR in K562 cells for both daunorubicin and doxorubicin a decrease in both lipid and nucleic acid conponents with an increase in the protein content was observed. However our study clearly indicates an increase in the lipid/protein ratio indication a lipidation in the resistant cell lines. The contrasting results of these studies indicate that the metabolic consequences of the resistance differs significantly with different drugs used.

There were changes in the shapes of the Amide I and II bands as seen in Figure 6. Since Amide I band frequency and shape is sensitive to protein conformation, this shifting and shape changes are attributed to the changes in protein conformation (47). The intensity ratio of Amide I/Amide II is another measure of protein conformational changes. This ratio was found to increase 16.95% for K562/NIL-50 cells indicating protein secondary structural changes. In a study by Zhou *et al*. in HL60 cells that underwent apoptosis, this ratio was also found to increase. Although this ratio was ascribed to the changes in only membrane proteins, in this study it describes a total change in the proteome and protein structural changes of that proteome (48). The secondary structural analysis using the second derivative of Amide I

band supported these observations. A protein kinase inhibitor can change the cellular metabolism in a variety of ways. For example, as a toxic compound a kinase inhibitor can initiate Endoplasmic Reticulum stress response causing expression of new proteins (chaperones and Heat Shock Proteins) in the cell to protect the cellular proteins from denaturation. The presence of cellular stress condition can alter gene expression profiles significantly. Therefore the proteome of the sensitive and resistant cells differ very much (49). This differentiation in the proteome causes changes in the average secondary structures of sensitive and resistant cells accordingly. In a study (13) Le Gal (1993) *et al.* considered the effect of MDR (doxorubicin) on the Amide I and II bands of K562 cells and their study are parallel to ours in that we both observed a significant increase in the band around 1690 cm^{-1} (antiparallel beta sheets).

The bands at 1239 cm^{-1}, 1086 cm^{-1} and 970 cm^{-1} are nucleic acid bands. The 1239 cm^{-1} band is due to asymmetric phosphate stretching and the 1086 cm^{-1} band is due to symmetric phosphate stretching band of nucleic acids (30, 31). The band at 970 cm^{-1} is due to C-N^{+}-C stretching of nucleic acids (33). The frequency of the symmetric stretching band was shifted to lower frequency values in nilotinib resistant cells. In addition the intensities of the bands at 1239 and 970 cm^{-1} were lower for nilotinib resistant cells which indicates changes in the relative amount of nucleic acids and structural changes in nuclear morphology, organization, and architecture. These changes include alterations in the nuclear/cytoplasmic ratio, hyperchromacity, chromatin aggregation and changes in DNA condensation between nilotinib sensitive and resistant K562 cells. In a study by McNamara *et al*. (2008) resistance of acute promyelocytic leukemia cells to retinoic acid was associated with changes in the expression level of topoisomerase II beta (50). Similarly multi drug resistance was linked to specific nuclear morphological changes acquired in the process of selection by cytotoxic drugs rather than P-gp overexpression (51).

The intensity ratio of the 1086 cm^{-1} band which is due to symmetric phosphate stretching of nucleic acids and the Amide II band at 1545 cm^{-1} is used to estimate DNA/protein ratio in the cellular systems investigated (52). In this study the intensity ratio of 1080 cm^{-1} and Amide II bands increased by 2.78% in K562/NIL-50 cells indicating a small increase in the DNA over protein amount. Similar increases in this ratio were observed in differentiated and apoptotic cells (49). Benedetti *et al.* (1988) and Gaigneaux *et al.* (2002) found a similar trend of increase in DNA/protein content in chronic lymphatic leukemia cells during cellular differentiation (12, 53).

Glucose/phosphate is a reliable measure for metabolic turnover of the cells (54) and it is indicated by the intensity ratio of the 1030 cm^{-1} and 1086 cm^{-1} bands. The glucose/phosphate ratio was found to increase by 21% in K562/NIL-50 cells. In earlier studies, the phosphate level was higher for normal cells and carbohydrate levels also showed a corresponding increase in H-ras transfected malignant cells (54). Similarly, the intensity ratio of 1030 cm^{-1} and 2926 cm^{-1} bands was found to increase by 17.24% in K562/NIL-50 cells. This ratio is indicative of the ratio of glucose/phospholipids and is a measure of de novo synthesis of phospholipids at the expense of free glucose in the cell (54). This ratio was found to be larger for normal cells as compared to those transformed by H-ras. The phospholipid molecules and their metabolites are believed to participate in the oncogene-induced transformation processes (55). Similarly, it was reported that all phospholipid fractions were reduced in *ras*-transfected fibroblasts except phosphotidylethanolamine (56). These results that phosphate content is higher in normal cells than in the *ras* transfected cell lines are in agreement with our results for nilotinib resistant K562 cells. In a study by Gazi *et al*. the intensity ratio of the 1030 cm^{-1} and 1086 cm^{-1} bands was interpreted as glycogen-to-phosphate ratio and proposed as a marker for cancer to distinguish benign and malignant prostate cancer and they concluded that the ratio decreased in malignant tissue (57). Their findings indicate a close connection between carbohydrate and lipid metabolisms in the development of malignant cancer cells and the subject should be investigated metabolically.

A significant decrease (20.11%) in the intensity ratio of the 1121 cm^{-1} and 1020 cm^{-1} bands was observed in K562/NIL-50 cells. This ratio is often used as an index of cellular RNA/DNA ratio and is found to increase from normal to malignant cells (54). In this study, this ratio was found to decrease as opposed to the malignant transformation indicating the different biochemical natures of resistance formation and malignant transformation. It is also interesting to note that there was a negative correlation between the RNA/DNA and glucose/phosphate ratios. This is considered to be a good indicator to identify the transforming status of the cells. This can also be applied to tissues in the diagnosis of various types of malignancy in differentiating normal and cancerous cells.

The intensity ratio of the band at 1121 cm^{-1} and Amide II bands increased by 5.18% in K562/NIL-50 cells. This ratio gives an idea about the transcriptional status of the cell. In H-ras transfected cells, high variation of this ratio for ras-transfected malignant cells remained unresolved (54). The results indicate that the transcriptional status of the K562/NIL-50 cells increases.

In cancer therapy a number of different drugs are in use. Since many of them have been known to raise drug resistance phenomena, a detailed analysis of the comparative effects of these drugs in the same cell lines should be carried out using FT-IR technique. In addition since the nature of each

type of cancer may be different because of their different cell types and causative agent, it may be difficult to make generalizations about the nature of metabolic differences between resistance behaviors. Similarly, different mechanisms cause drug resistance in cancer cells. Therefore comprehensive molecular and spectroscopic studies should be carried out to make generalizations about the onset and progress of cancer and resistance behavior of cancer cells against these drugs. Finally, since the only experimental method to investigate the metabolic rate data is the FTIR technique here, other experimental methods should be used to correlate the results.

Conclusion

The results of the present study indicate that the induction of nilotinib resistance in K562 cells caused significant alterations in cellular structure. The content of glycogen was found to increase in the K562/NIL-50 cells as compared to parental cells. The amount of unsaturated lipids increased in the nilotinib resistant cells indicating lipid peroxidation. In addition, lipid membrane order was found to increase in the K562/NIL-50 cells. Although the total proportion of cholesterol and triglycerides to protein did not change significantly, nilotinib resistance caused significant changes in the cholesterol and triglyceride proportions in the cellular structures indicating possible changes in neutral lipid and lipid droplet metabolism as well as phospholipid metabolism which affect cell membrane structure. The relative content of nucleic acids did not change significantly with respect to protein content but structural/organizational changes in the nucleus were evident as revealed by frequency changes in the nucleic acid bands. Changes in the amide bands revealed changes in the proteome of the resistant cells. The alpha helix structure and random coil structure decreased, however, anti-parallel beta sheet structure, beta sheet structure and turns structure increased. The transcriptional status of DNA was found to decrease along with higher metabolic turn-over in the resistant cells. The results of the present study also revealed that FT-IR spectroscopy has the potential to be used as an analytical method of detecting and monitoring structural and functional changes in CML.

Conflict of Interest

The authors do not have any kind of conflict of interest affecting the current study.

Acknowledgements

We thank Prof Dr Anne Frary for for critically reviewing the manuscript and the staff of İzmir Institute of Technology, Department of Chemistry and Biotechnology and Bioengineering Center for their help and technical support. This study was supported by TUBITAK project number 107S317 to Y.B. and by the Turkish Academy of Sciences, Outstanding Young Investigator Programme to Y.B.

References

1. O'Hare, T., Walters, D. K., Deininger, M. W., Druker, B. J. AMN107: tightening the grip of imatinib. *Cancer Cell 7*, 117-119 (2005).
2. Frazer, R., Irvine, A. E., McMullin, M. F. Chronic Myeloid Leukaemia in The 21st Century. *Ulster Med J 76*, 8-17 (2007).
3. Weisberg, E., Manley, P., Mestan, J., Cowan-Jacob, S., Ray, A., Griffin, J. D. AMN107 (nilotinib): a novel and selective inhibitor of BCR-ABL. *Br J Cancer 94*, 1765-1769 (2006).
4. Kantarjian, H., Giles, F., Wunderle, L., Bhalla, K., O'Brien, S., Wassman, B., Tanaka, C., Manley, P., Rae, P., Mietlowski, W., Bochinski, K., Hochhaus, A., Griffin, J. D., Hoelzer, D., Albitar, M., Dugan, M., Cortes, J., Alland, L., Ottman, O. G. Nilotinib in imatinib-resistant CML and Philadelphia chromosome-positive ALL. *N Engl J Med 354*, 2542-2551 (2006).
5. Soverini, S., Gnani, A., Colarossi, S., Castagnetti, F., Abruzzese, E., Paolini, S., Merante, S., Orlandi, E., de Matteis, S., Gozzini, A., Iacobucci, I., Palandri, F., Gugliotta, G., Papayannidis, C., Poerio, A., Amabile, M., Cilloni, D., Rosti, G., Baccarani, M., Martinelli, G. Philadelphia-positive patients who already harbor imatinib-resistant Bcr-Abl kinase domain mutations have a higher likelihood of developing additional mutations associated with resistance to second- or third-line tyrosine kinase inhibitors. *Blood 114*, 2168-71 (2009).
6. Ray, A., Cowan-Jacob, S. W., Manley, P. W., Mestan, J., Griffin, J. D. Identification of BCR-ABL point mutations conferring resistance to the Abl kinase inhibitor AMN107 (nilotinib) by a random mutagenesis study. *Blood 109*, 5011-5 (2007).
7. Dogan, A., Ergen, K., Budak, F., Severcan, F. Evaluation of disseminated candidiasis on an experimental animal model: a fourier transform infrared study. *Appl Spectrosc 61*, 199-203 (2007).
8. Cakmak, G., Togan, I., Severcan, F. 17Beta-estradiol induced compositional, structural and functional changes in rainbow trout liver, revealed by FT-IR spectroscopy: a comparative study with nonylphenol. *Aquat Toxicol 77*, 53-63 (2006).
9. Toyran, N., Zorlu, F., Severcan, F. Effect of stereotactic radiosurgery on lipids and proteins of normal and hypoperfused rat brain homogenates: a Fourier transform infrared spectroscopy study. *Int J Radiat Biol 81*, 911-918 (2005).
10. Yano, K., Ohoshima, S., Gotou, Y., Kumaido, K., Moriguchi, T., Katayama, H. Direct measurement of human lung cancerous and non-cancerous tissues by fourier transform infrared microscopy: can an infrared microscope be used as a clinical tool? *Anal Biochem 287*, 218-225 (2000).
11. Lewis, P. D., Lewis, K. E., Ghosal, R., Bayliss, S., Lloyd, A. J., Wills, J., Godfrey, R., Kloer, P., Mur, L. A. Evaluation of FTIR spectroscopy as a diagnostic tool for lung cancer using sputum. *BMC Cancer 10*, 640 (2010).
12. Gaigneaux, A., Ruysschaert, J. M., Goormaghtigh, E. Infrared spectroscopy as a tool for discrimination between sensitive and multiresistant K562 cells. *Eur J Biochem 269*, 1968-1973 (2002).
13. Le Gal, J. M., Morjani, H., Manfait, M. Ultrastructural appraisal of the multidrug resistance in K562 and LR73 cell lines from Fourier transform infrared spectroscopy. *Cancer Res 53*, 3681-3686 (1993).
14. Piskin, O., Ozcan, M. A., Ozsan, G. H., Ates, H., Demirkan, F., Alacacioglu, I., Undar, B. Synergistic effect of imatinib mesylate and fludarabine combination on Philadelphia chromosome-positive chronic myeloid leukemia cell lines. *Turk J Haematol 24*, 23-27 (2007).
15. Garip, S., Yapici, E., Ozek, N. S., Severcan, M., Severcan F., Evaluation and discrimination of sivastatin-induced structural alterations in proteins of different rat tissues by FTIR spectroscopy and neural network analysis. *Analyst 135*, 3233-3241 (2010).

16. Melin, A. M., Perromat, A., Deleris, G. Pharmacologic application of fourier transform IR spectroscopy: in vivo toxicity of carbon tetrachloride on rat liver. *Biopolymers 57*, 160-168 (2000).
17. Ozek, N. S., Tuna, S. T., Erson-Bensan, E., Severcan, F. Characterization of microRNA-125b expression in MCF7 breast cancer cells, *Analyst 135*, 3094-3102 (2010).
18. Cakmak, G., Zorlu, F., Severcan, M., Severcan, F. Screening of protective effect of amifostine on radiation-induced structural and functional variations in rat liver microsomal membranes by FT-IR spectroscopy. *Anal Chem 83*, 2438-2444 (2011).
19. Elibol-Can, B., Jabukowska-Dogru, E., Severcan, M., Severcan, F. The Effects of Short-Term Chronic Ethanol Intoxication and Ethanol Withdrawal on the Molecular Composition of the Rat Hippocampus by FT-IR Spectroscopy, *Alcohol Clin Exp Res 35*, 1-13 (2011).
20. Jamin, N., Dumas, P., Moncuit, J., Fridman, W. H., Teillaud, J. L., Carr, G. L., Williams, G. P. Highly resolved chemical imaging of living cells by using synchrotron infrared microspectrometry. *Proc Natl Acad Sci U S A 95*, 4837-4840 (1998).
21. Dovbeshko, G. I., Gridina, N. Y., Kruglova, E. B., Pashchuk, O. P. FTIR spectroscopy studies of nucleic acid damage. *Talanta 53*, 233-246 (2000).
22. Lyman, D. J., Murray-Wijelath, J. Vascular graft healing: I. FTIR analysis of an implant model for studying the healing of a vascular graft. *J Biomed Mater Res 48*, 172-186 (1999).
23. Chan, S. I., Bocian, D. F., Petersen, N. O. Nuclear Magnetic Resonance Studies of the Phospholipid Bilayer Membrane in Membrane Spectroscopy. *Grell, E. (Ed.)*, Springer Verlag, Heidelberg (1981).
24. Takahashi, H., French, S. W., Wong, P. T. Alterations in hepatic lipids and proteins by chronic ethanol intake: a high-pressure Fourier transform infrared spectroscopic study on alcoholic liver disease in the rat. *Alcohol Clin Exp Res 15*, 219-223 (1991).
25. Gasper, R., Dewelle, J., Kiss, R., Mijatovic, T., Goormaghtigh, E. IR spectroscopy as a new tool for evidencing antitumor drug signatures. *Biochim Biophys Acta 1788*, 1263-1270 (2009).
26. Nara, M., Okazaki, M., Kagi, H. Infrared study of human serum very-low-density and low-density lipoproteins. Implication of esterified lipid C=O stretching bands for characterizing lipoproteins. *Chem Phys Lipids 117*, 1-6 (2002).
27. Voortman, G., Gerrits, J., Altavilla, M., Hening, M., van Bergeijk, L., Hessels, J. Quantitative determination of faecal fatty acids and triglycerides by Fourier transform infrared analysis with a sodium chloride transmission flow cell. *Clin Chem Lab Med 40*, 795-798 (2002).
28. Manoharan, R., Baraga, J. J., Rava, R. P., Dasari, R. R., Fitzmaurice, M., Feld, M. S. Biochemical analysis and mapping of atherosclerotic human artery using FT-IR microspectroscopy. *Atherosclerosis 103*, 181-193 (1993).
29. Jackson, M., Ramjiawan, B., Hewko, M., Mantsch, H. H. Infrared microscopic functional group mapping and spectral clustering analysis of hypercholesterolemic rabbit liver. *Cell Mol Biol (Noisy-le-grand) 44*, 89-98 (1998).
30. Wong, P. T. T., Papavassiliou, E. D., Rigas, B. Phosphodiester Stretching Bands in the Infrared-Spectra of Human Tissues and Cultured-Cells. *Applied Spectroscopy 45*, 1563-1567 (1991).
31. Wang, J. J., Chi, C. W., Lin, S. Y., Chern, Y. T. Conformational changes in gastric carcinoma cell membrane protein correlated to cell viability after treatment with adamantyl maleimide. *Anticancer Res 17*, 3473-3477 (1997).
32. Chiriboga, L., Yee, M., Diem, M. Infrared spectroscopy of human cells and tissue. Part VI: A comparative study of histopathology and infrared microspectroscopy of normal, cirrhotic, and cancerous liver tissue. *Applied Spectroscopy 54*, 1-8 (2000).
33. Ci, Y. X., Gao, T. Y., Feng, J., Guo, Z. Q. Fourier transform infrared spectroscopic characterization of human breast tissue: Implications for breast cancer diagnosis. *Applied Spectroscopy 53*, 312-315 (1999).
34. Mahon, F. X., Hayette, S., Lagarde, V., Belloc, F., Turcq, B., Nicolini, F., Belanger, C., Manley, P. W., Leroy, C., Etiene, G., Roche, S., Pasquet, J. M. Evidence that resistance to nilotinib may be due to BCR-ABL, Pgp, or Src kinase overexpression. *Cancer Res 68*, 9809-16 (2008).
35. Baran, Y., Salas, A., Senkal, C. E., Gunduz, U., Bielawski, J., Obeid, L. M., Ogretmen, B. Alterations of ceramide/sphingosine 1-phosphate rheostat involved in the regulation of resistance to imatinib-induced apoptosis in K562 human chronic myeloid leukemia cells. *J Biol Chem 282*, 10922-10934 (2007).
36. Mourant, J. R., Gibson, R. R., Johnson, T. M., Carpenter, S., Short, K. W., Yamada, Y. R., Freyer, J. P. Methods for measuring the infrared spectra of biological cells. *Phys Med Biol 48*, 243-257 (2003).
37. Kim, H. H., Kim, T., Kim, E., Park, J. K., Park, S. J., Joo, H. The mitochondrial Warburg effect: a cancer enigma. *Interdisciplinary Bio Central 1*, 1-7 (2009).
38. Xia, S., Yu, S., Yuan, X. Effects of hypoxia on expression of P-gp and mutltidrug resistance protein in human lung adenocarcinoma A549 cell line. *J Huazhong Univ Sci Technolog Med Sci 25*, 279-281 (2005).
39. Xu, R. H., Pelicano, H., Zhou, Y., Carew, J. S., Feng, L., Bhalla, K. N., Keating, M. J., Huang, P. Inhibition of glycolysis in cancer cells: a novel strategy to overcome drug resistance associated with mitochondrial respiratory defect and hypoxia. *Cancer Res 65*, 613-621 (2005).
40. Pescador, N., Villar, D., Cifuentes, D., Garcia-Rocha, M., Ortiz-Barahona, A., Vazquez, S., Ordonez, A., Cuevas, Y., Saez-Morales, D., Garcia-Bermejo, M. L., Landazuri, M. O., Guinovart, L. del Peso J. Hypoxia promotes glycogen accumulation through hypoxia inducible factor (HIF)-mediated induction of glycogen synthase 1. *PLoS One 5*, e9644 (2010).
41. Severcan, F., Gorgulu, G., Gorgulu, S. T., Guray, T. Rapid monitoring of diabetes-induced lipid peroxidation by Fourier transform infrared spectroscopy: evidence from rat liver microsomal membranes. *Anal Biochem 339*, 36-40 (2005).
42. Schuldes, H., Dolderer, J. H., Zimmer, G., Knobloch, J., Bickeboller, R., Jonas, D., Woodcock, B. G. Reversal of multidrug resistance and increase in plasma membrane fluidity in CHO cells with R-verapamil and bile salts. *Eur J Cancer 37*, 660-667 (2001).
43. Dolderer, J. H., Zimmer, G., Woodcock, B. G., Bockhorn, H., Bickeböller, R., Schuldes, H. Resistance modulation in CHO cells by R-verapamil and bile salts is associated with physical and chemical changes in the cell membrane, *Int J Clin Pharmacol Ther 38*, 196-203 (2000).
44. Tsvetkova, N. M., Horvath, I., Torok, Z., Wolkers, W. F., Balogi, Z., Shigapova, N., Crowe, L. M., Tablin, F., Vierling, E., Crowe, J. H., Vigh, L. Small heat-shock proteins regulate membrane lipid polymorphism. *Proc Natl Acad Sci USA 99*, 13504-13509 (2002).
45. Lavie, Y., Fiucci, G., Czarny, M., Liscovitch, M. Changes in membrane microdomains and caveolae constituents in multidrug-resistant cancer cells. *Lipids 34 Suppl*, S57-63 (1999).
46. Manechez, A., Reungpatthanaphong, P., de Certaines, J. D., Leray, G., Le Moyec, L. Proton NMR visible mobile lipid signals in sensitive and multidrug-resistant K562 cells are modulated by rafts. *Cancer Cell Int 5*, 2 (2005).
47. Jackson, M., Mansfield, J. R., Dolenko, B., Somorjai, R. L., Mantsch, H. H., Watson, P. H. Classification of breast tumors by grade and steroid receptor status using pattern recognition analysis of infrared spectra. *Cancer Detect Prev 23*, 245-253 (1999).
48. Zhou, J., Wang, Z., Sun, S., Liu, M., Zhang, H. A rapid method for detecting conformational changes during differentiation and apoptosis of HL60 cells by Fourier-transform infrared spectroscopy. *Biotechnol Appl Biochem 33*, 127-132 (2001).
49. Pocaly, M., Lagarde, V., Etienne, G., Dupouy, M., Lapaillerie, D., Claverol, S., Vilain, S., Bonneu, M., Turcq, B., Mahon, F. X.,

Pasquet, J. M. Proteomic analysis of an imatinib-resistant K562 cell line highlights opposing roles of heat shock cognate 70 and heat shock 70 proteins in resistance, *Proteomics 8*, 2394-2406 (2008).
50. McNamara, S., Miller, Jr. W. H. Expanding the use of retinoids in acute myeloid leukemia: spotlight on bexarotene. *Clin Cancer Res 14*, 5311-5313 (2008).
51. Dufer, J., Millot-Broglio, C., Oum'Hamed, Z., Liautaud-Roger, F., Joly, P., Desplaces, A., Jardillier, J. C. Nuclear DNA content and chromatin texture in multidrug-resistant human leukemic cell lines. *Int J Cancer 60*, 108-114 (1995).
52. Mourant, J. R., Yamada, Y. R., Carpenter, S., Dominique, L. R., Freyer, J. P. FTIR spectroscopy demonstrates biochemical differences in mammalian cell cultures at different growth stages. *Biophys J 85*, 1938-1947 (2003).
53. Benedetti, E., Vergamini, P., Spremolla, G. Ft-Ir Analysis of Single Human Normal and Leukemic Lymphocytes. *Mikrochimica Acta 1*, 139-141 (1988).
54. Ramesh, J., Salman, A., Hammody, Z., Cohen, B., Gopas, J., Grossman, N., Mordechai, S. Application of FTIR microscopy for the characterization of malignancy: H-ras transfected murine fibroblasts as an example. *J Biochem Biophys Methods 50*, 33-42 (2001).
55. Carnero, A., Cuadrado, A., Dolfi, F., Jimenez, B., Delpeso, L., Esteve, P., Montaner, S., Embade, N., Ramos, A., Lacal, J. C. Regulation of Phospholipid-Metabolism by Ras Proteins. *Gtpase-Controlled Molecular Machines 6*, 321-340 (1994).
56. Momchilova, A., Markovska, T., Pankov, R. Ha-ras-transformation alters the metabolism of phosphatidylethanolamine and phosphatidylcholine in NIH 3T3 fibroblasts. *Cell Biol Int 23*, 603-610 (1999).
57. Gazi, E., Dwyer, J., Gardner, P., Ghanbari-Siahkali, A., Wade, A. P., Miyan, J., Lockyer, N. P., Vickerman, J. C., Clarke, N. W., Shanks, J. H., Scott, L. J., Hart, C. A., Brown, M. Applications of Fourier transform infrared microspectroscopy in studies of benign prostate and prostate cancer. A pilot study. *J Pathol 201*, 99-108 (2003).

Received: January 6, 2012; Revised: May 24, 2012;
Accepted: May 25, 2012